Spectral Analysis of Phase Noise in Bipolar LC-Oscillators—Theory, Verification, and Design

Aleksandar Tasić, Wouter A. Serdijn, and John R. Long

***Abstract*—Interpretation of phase-noise generating mechanism in oscillators relies on approximate and numerical calculations for analysis, and simulation tools for synthesis. In this paper, a comprehensive, yet intuitive, phase-noise model is derived as a function of oscillator circuit parameters, suiting both analysis and synthesis of oscillators. Contributions of all noise sources to the phase noise of bipolar inductance–capacitance (*LC*) voltage-controlled oscillators have been determined using spectral noise analysis. For the verification of the phase-noise model, a bipolar *LC*-oscillator has been designed that realizes a phase noise of −106 dBc/Hz at 1 MHz offset from a 5.7 GHz-band carrier while drawing 4.8 mA from a 2.2 V supply. The results obtained from the phase-noise model agree well with simulation and measurement results of the *LC*-oscillator designed.**

***Index Terms*—Duty cycle, noise factor, noise folding, phase noise, small-signal loop gain, voltage-controlled oscillator (VCO).**

I. Introduction

INTERPRETATIONS of the mechanism of phase-noise generation in oscillators are bounded to approximations and numerical calculations [1]–[8]. The phase-noise models obtained are often only indicative, failing to describe the oscillator phase noise using circuit parameters. Computer-aided simulation tools are therefore indispensable not only for synthesis but also for analysis of the oscillator performance.

In this paper, we introduce an intuitive, yet simple, phase-noise model for inductance–capacitance (*LC*) voltage-controlled oscillators (VCOs) using spectral noise analysis. It is amenable for design as it describes the noise performance of *LC* voltage-controlled oscillators qualitatively and quantitatively using electrical parameters.

Noise contributions to the phase noise of the *LC*-tank, transconductor (g_m-cell), and bias circuitry are determined for bipolar *LC* oscillators in this paper. The bias current-source noise of bipolar *LC*-VCOs is shown analytically to be larger than all other noise contributions put together (i.e., *LC*-tank noise and transconductor noise), in high-performance oscillator circuits [9], [10].

For the verification of the phase-noise model derived, a bipolar *LC* VCO has been designed. The oscillator simulation and measurement results have been shown to comply with the theoretical calculation results obtained from the phase-noise analysis method proposed.

A generic oscillator phase-noise model is described in the following section of this paper. Oscillator time-varying transfer functions are determined in Section III. Using spectral analysis of noise in oscillators, the contributions of all the noise sources to the phase noise are determined for bipolar *LC*-VCOs in Section IV, and the noise factors of the *LC*-tank, transconductor, and bias current source formulated. The phase-noise model derived is verified in Section V by comparing the theoretical and simulation results for the bipolar *LC*-oscillator. The test *LC*-oscillator circuit parameters and experimental results are presented in Section VI, confirming the validity of the phase-noise model. Paper is concluded in Section VII.

II. Generic Phase-Noise Model

In this paper, we will refer to the Bennett noise representation model [11], stating that if a signal is characterized by a single-sided power spectral density of N, then the amplitude of its component at a given frequency has a value of $\sqrt{2N}$. The relationships between single-sided and double-sided power spectral densities and corresponding Fourier magnitude components according to this model can be described as follows: for a $4KTR = N$ single-sided noise power spectral density of a resistor R, the noise signal magnitude at an arbitrary frequency f_0 of a polar Fourier development (positive frequencies) is $\sqrt{8KTR}$ (i.e, $\sqrt{2N}$), and of a complex Fourier development (positive and negative frequencies) is $\sqrt{2KTR}$ (i.e., $\sqrt{N/2}$) [12], T being the absolute temperature, and K Boltzmann's constant.

Fig. 1(a) shows a block diagram of an *LC*-oscillator with a resonating *LC*-tank and a (nonlinear, limiting) cross-coupled transconductance amplifier (i.e., g_m-cell) in a positive feedback configuration over a voltage divider $(/n)$.

v_N, $i_{N,O}$ and $v_{N,O}$ are the Fourier amplitude components of noise signals at the inputs of the transconductance amplifier, resonator, and feedback divider, respectively. For the amplitude of the signal current $i_S = v_S/R_{TK}$ through the resonator, the phasor diagram shown in Fig. 1(b) illustrates the relationship between the noise component at a frequency $f_0 + \Delta$ and the oscillation signal at a frequency f_0. v_S is the amplitude of the oscillation voltage signal across the *LC*-tank, R_{TK} the *LC*-tank parallel loss resistance at resonance, f_0 the oscillation (resonant) frequency, and Δ the offset frequency. *For the sake of a simpler notation, we treat as positive, by nature alternating phase-modulating components and noise conversion coefficients in the following analysis.*

Referred to the oscillation signal component i_S, the noise component $i_{N,O}$ can be split into an in-phase i_{AM}

Manuscript received December 31, 2008; revised April 03, 2009. First published June 19, 2009; current version published April 09, 2010. This paper was recommended by Associate Editor J. Silva-Martinez.

A. Tasić is with Qualcomm, San Diego, CA 92121 USA (e-mail: atasic@qualcomm.com).

W. A. Serdijn and J. R. Long are with the Electronics Research Laboratory/DIMES, Delft University of Technology, Delft 2628CD, The Netherlands.

Digital Object Identifier 10.1109/TCSI.2009.2025814

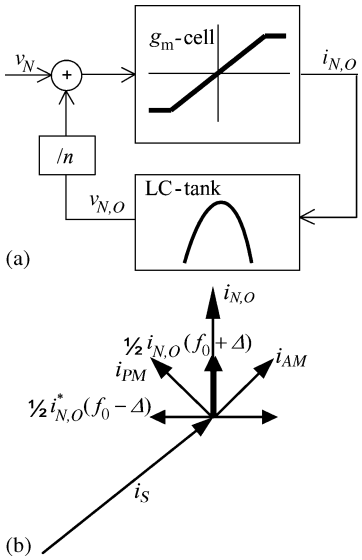

Fig. 1. (a) Oscillator positive-feedback model. (b) Phasor description of oscillator phase-noise model (counter-clockwise rotation).

(amplitude-modulating-AM) and a quadrature-phase i_{PM} (phase-modulating-PM) component. Referred to the noise component $i_{N,O}$, the PM and AM noise components are split into two noise components, each, at frequencies $f_0 + \Delta$ and $f_0 - \Delta$, respectively, as shown in Fig. 1(b). The in-phase AM noise component can be easily removed by the amplitude limiting mechanism of the cross-coupled amplifier [13]. However, the quadrature PM noise component is unavoidable, being the main concern to oscillator designers.

From Fig. 1(b) and a conjugate-component relationship $i^*_{N,O}(f_0 - \Delta) = i_{N,O}(-f_0 + \Delta)$ [14], the double-sided phase-modulating noise component at a frequency $f_0 + \Delta$ can be determined as

$$i_{PM}(f_0+\Delta) = \frac{1}{2}\left[i_{N,O}(f_0+\Delta) + i_{N,O}(-f_0+\Delta)\right] \quad (1)$$

describing the contribution of the noise components at an offset frequency Δ from positive and negative oscillation frequencies $\pm f_0$ to the PM noise component at $f_0 + \Delta$.

Similarly, the double-sided phase-modulating noise component at a frequency $-f_0 - \Delta$ is determined as

$$i_{PM}(-f_0-\Delta) = \frac{1}{2}\left[i_{N,O}(-f_0-\Delta) + i_{N,O}(f_0-\Delta)\right]. \quad (2)$$

A single-sided phase-modulating component is now obtained by folding the PM noise magnitudes from positive to negative frequencies and combining them. In other words, *a single-sided phase-modulating noise component at $f_0 + \Delta$ is obtained by summing one half of the double-sided contributions of the noise components at frequencies $\pm f_0 \pm \Delta$.*

The single-sided phase-related noise power (i.e., phase-related noise power density) is now determined combining the magnitudes of the spectral components of (1), (2) as $i_{PM,\mathrm{TOT}}$,

$$i^2_{PM,\mathrm{TOT}}(f_0+\Delta) = \frac{1}{2}\left[i_{PM}(f_0+\Delta) + i_{PM}(-f_0-\Delta)\right]^2 \quad (3)$$

where the magnitudes of correlated components are summed before their rms power is calculated.

Finally, the phase-related noise power density (thus referred to a 1 Hz bandwidth) relates to the single-sided phase noise ($\mathcal{L}$) at the output of the resonator at a frequency $f_0 + \Delta$ as

$$\mathcal{L} = \frac{|Z(f_0+\Delta)|^2\, i^2_{PM,\mathrm{TOT}}}{v_S^2/2}. \quad (4)$$

$Z(f_0 + \Delta f)$ is the equivalent *LC*-tank impedance at an offset frequency Δ from the resonant frequency f_0.

This is a well known phase-noise formulation, being the ratio of the noise power in a 1 Hz bandwidth at frequency $f_0 + \Delta$ and the carrier power at frequency f_0 [2]. For the oscillator model shown in Fig. 1(a) it reads

$$\mathcal{L} = \frac{v^2_{PM,\mathrm{TOT}}}{v_S^2/2}, \quad v^2_{PM,\mathrm{TOT}} = |Z(f_0+\Delta)|^2\, i^2_{PM,\mathrm{TOT}} \quad (5)$$

where $v^2_{PM,\mathrm{TOT}}$ stands for the total voltage noise spectral density at the output of the oscillator (i.e., across the LC-tank).

In the remainder of this paper, the oscillator phase noise will be determined using the model shown in Fig. 1(a) and [(1)–(5)].

The transformations of the oscillator noise sources to the *LC*-tank ($i_{PM,\mathrm{TOT}}$) must be known for an estimation of the oscillator phase noise. Considering the transconductor as a nonlinear voltage-to-current converter (i.e., limiter) [14] allows for the inclusion of all the noise generating mechanisms in *LC*-oscillators. By this, phenomena such as modulation of the transconductor noise and switching the noise of the bias current source, both resulting in the folding of noise [6], [14], can be described.

Before calculating the phase noise of *LC*-oscillators using the spectral noise analysis method, we will derive the Fourier series for the time-varying small-signal g_m-cell gain and the g_m-cell switching characteristic for a bipolar *LC*-oscillator. The results obtained are general and apply to CMOS *LC*-oscillators as well.

III. Bipolar *LC*-Oscillators Time-Varying Transfer Functions

The voltage-controlled oscillator shown in Fig. 2 is used for the phase-noise analysis of bipolar *LC*-oscillators. It consists of a resonant *LC* tank, a capacitive voltage divider (C_A, C_B), and a cross-coupled transconductance amplifier (Q_1, Q_2). The bias current source provides current I_{TAIL}.

This VCO is a second-order (negative resistance) oscillator in a positive feedback configuration between the resonant *LC*-tank and the transconductor via the capacitive divider. The oscillation condition is satisfied when the *LC*-tank loss conductance is compensated by the equivalent negative small-signal transconductance of the transconductance amplifier.

The relationships between the parameters of the oscillator are summarized by (6)–(8). L is the tank inductance, C the tank capacitance, G_{TK} ($1/R_{TK}$) the effective tank conductance, R_L and R_C the series loss resistances of the resonator inductor and capacitor, respectively, n the capacitive divider ratio, g_m the transconductance of bipolar transistors Q_1, Q_2, C_π their base-emitter capacitance, k the small-signal loop gain, V_T the thermal voltage, and ω_0 the oscillation angular frequency [15]

$$G_{TK} = \frac{R_L}{(\omega_0 L)^2} + R_C(\omega_0 C)^2 \quad (6)$$

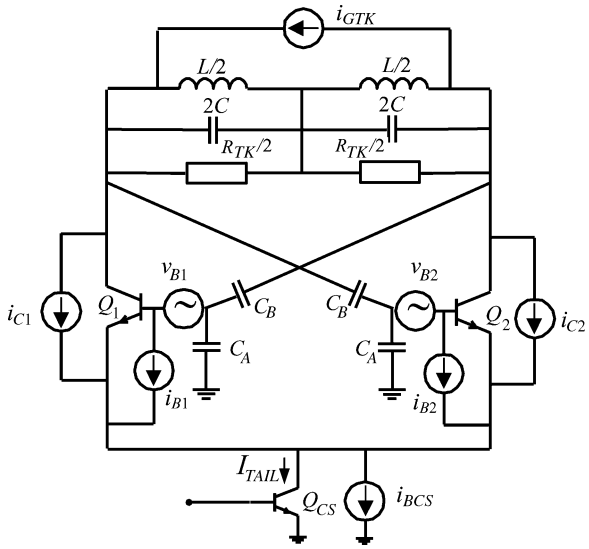

Fig. 2. Bipolar *LC*-VCO and its main noise sources (bias not completed).

$$k=\frac{g_m}{2n}\frac{1}{G_{TK}} \quad g_m=\frac{I_{\rm TAIL}}{2V_T} \quad n=1+\frac{C_A+C_\pi}{C_B} \tag{7}$$

$$\omega_0=\frac{1}{\sqrt{LC_{\rm TOT}}} \quad C_{\rm TOT}=C+\frac{1}{2}\frac{(C_A+C_\pi)C_B}{C_A+C_\pi+C_B}. \tag{8}$$

The double-sided noise power densities of the oscillator noise sources shown in Fig. 2 are given by (9)–(12). These are the tank-conductance current noise (symbol i_{GTK} and rms value $i_N(G_{TK})$), the base-resistance (r_B) thermal noise (symbol v_B and rms value $v_N(r_B)$), the collector-current shot noise (symbol i_C and rms value $i_N(I_C)$), and the base-current shot noise (symbol i_B and rms value $i_N(I_B)$), and the equivalent output current noise (symbol i_{BCS} and rms value $i_N(I_{BCS})$) of the current source transistor Q_{CS}

$$i_N^2(G_{TK})=2KTG_{TK} \tag{9}$$

$$v_N^2(r_B)=2KTr_B \tag{10}$$

$$i_N^2(I_C)=qI_C=\frac{2KTg_m}{2} \quad i_N^2(I_B)=qI_B=\frac{2KTg_m}{2\beta} \tag{11}$$

$$i_N^2(I_{BCS})=2KT\frac{g_{m,CS}}{2}[1+2r_{B,CS}g_{m,CS}]. \tag{12}$$

I_C and I_B stand for the collector and base currents and β for the current gain factor of the g_m-cell transistors, $g_{m,CS}$ is the transconductance and $r_{B,CS}$ the base resistance of transistor Q_{CS}.

A. Time-Varying Small-Signal g_m-Cell Gain

The nonlinear voltage-to-current transfer function (referred to the *LC*-tank) of the transconductor, its equivalent time-varying small-signal transconductance in the presence of a large driving signal, and the (large-signal) current through the resonator are shown in Fig. 3(a)–(c), respectively [14]. Two forms of otherwise hyperbolic-tangent V-to-I g_m-cell characteristic are used: a linear (dashed line) and a quadratic (solid line) approximation shown in Fig. 3(a), facilitating the description of the harmonic components of the waveforms in Fig. 3(b) and (c).

In this section, we will first compare the two V-to-I characteristics shown in Fig. 3(a) with the hyperbolic-tangent ($tanh$)

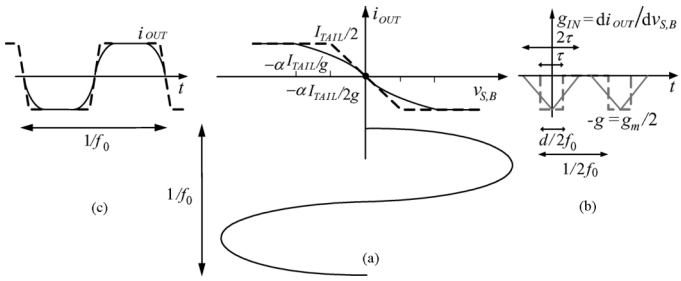

Fig. 3. (a) Large-signal V-to-I characteristic with (b) small-signal time-varying gain of the g_m-cell in the presence of a large drive signal and (c) (large signal) current through the resonator.

characteristic of the transconductor [see (13)] [6], and then use the one that describes the $tanh$ function more closely in the remainder of this paper

$$i_{\rm OUT}(t)=\frac{I_{\rm TAIL}}{2}tanh\left(\frac{v_{S,B}}{2V_T}\right). \tag{13}$$

$v_{S,B}$ is the voltage swing of the oscillation signal $v=v_{S,B}\sin\omega_0 t$ across the bases of the transconductor devices Q_1, Q_2, shown in Fig. 2.

In Fig. 3(b) are shown two approximate forms of the transconductor small-signal gain in the presence of a large oscillation signal: a square-wave (dashed line) and a triangular-wave (solid line) gain function.

As long as the oscillation signal (v) is not clipped, the gain of the accompanying noise signal has a constant value, g, for a square-wave function, and a linearly decaying value, starting from g, for a triangular-wave function. When limiting occurs, the small-signal gain reduces to zero. If the period of the oscillation signal is $1/f_0$, the period of the small-signal time-varying gain $(g_{\rm IN})$ is $1/(2f_0)$. Considering the transformation from the bases to the collectors of the transconductor Q_1-Q_2, the peak value of the small-signal gain g is $g_m/2$.

Let us now determine the average value and normalized power of the time-varying gain functions shown in Fig. 3(b), and compare them with the average value and the normalized power value of the time-varying gain originating from the $tanh$ transconductor characteristic, given by (13).

If d is the duty cycle and τ the width of the square-wave function $g_{\rm IN}(t)$ [see Fig. 3(b)], then the average values of the square-wave gain, $g_{\square,0}$, the triangular-wave gain, $g_{\triangledown,0}$, and the gain of the $tanh$ g_m-cell characteristic, $g_{th,0}$, are given by (14)–(16), respectively, $(T_2=0.5/f_0)$

$$g_{\square,0}=\frac{1}{T_2}\int_{-T_2/2}^{T_2/2}g_{\square}(t)dt=\frac{2}{T_2}\int_0^{\tau/2}gdt=g\frac{\tau}{T_2}=gd \tag{14}$$

$$g_{\triangledown,0}=\frac{1}{T_2}\int_{-T_2/2}^{T_2/2}g_{\triangledown}(t)dt=\frac{2}{T_2}\int_0^{\tau}g\left(1-\frac{t}{\tau}\right)dt=gd \tag{15}$$

$$g_{th,0}=\frac{1}{T_2}\int_{-T_2/2}^{T_2/2}g_{th}(t)dt=\frac{2}{\pi v_s}\int_0^{4V_T}\frac{\partial i_{\rm OUT}(v)}{\partial v}dv=\frac{I_{\rm TAIL}}{\pi v_{S,B}}. \tag{16}$$

Equation (16) is solved by exchanging the time integration variable with the oscillation signal $v = v_{S,B}\sin\omega_0 t$, and assuming $v_{S,B} \gg 4V_T$, i.e., the small-signal loop gain is much greater than 1.

In order to compare (14)–(16), let us first determine the duty cycle d of the dashed gain function, shown in Fig. 3(b). We also calculate the voltage swing across the resonator (and product gd), needed for the comparison of (14)–(16), and later for the derivation of the phase noise, according to (5).

If $\pm 2\xi V_T$ is the linear region of the piece-wise transconductor approximation [dashed V-to-I function of Fig. 3(a)], the duty cycle of the square-wave time-varying gain can be expressed as

$$d = \frac{2}{\pi}\arcsin\left(\frac{2\xi V_T}{v_{S,B}}\right). \tag{17}$$

The voltage swing across the *LC*-tank is defined as the product of the tank resistance $1/G_{TK}$ and the first Fourier coefficient of the current I_1 through the tank, $v_S = I_1 R_{TK}$.

For a large value of the oscillator small-signal loop gain k, output current $i_{\rm OUT}$ is described by a close-to-square wave with amplitude $I_{\rm TAIL}/2$ [see Fig. 3(c)]. Component I_1 now equals the first harmonic of the current signal shown. With the aid of (7), the voltage swing across the resonator v_S then reads

$$v_S = \frac{2}{\pi} I_{\rm TAIL} R_{TK} = \frac{8}{\pi} k n V_T = n v_{S,B}. \tag{18}$$

Assuming a 100 mV ($\pm 2V_T$) bipolar transconductor linear region (dashed line of Fig. 3(a), [14]) and a large small-signal loop-gain value, the duty cycle d of the square-wave gain function can be approximated as

$$d = \frac{4V_T}{\pi v_{S,B}} \tag{19}$$

or with the aid of (18) as

$$d = \frac{1}{2k}. \tag{20}$$

This expression describes the relationship between the small-signal loop gain and duty cycle for $k \gg 1$ (i.e., large oscillation signal generated and hard switching of the transconductor). The product gd now becomes [see (14)–(19)]

$$gd = \frac{I_{\rm TAIL}}{4V_T}\frac{4V_T}{\pi v_{S,B}} = \frac{I_{\rm TAIL}}{\pi v_{S,B}} \tag{21}$$

and the equality of the average values of (14)–(16) is due. The duty cycle d of the square-wave gain function shown in Fig. 3(b) can be now considered as the effective duty cycle of the triangular-wave gain function. Thus, both V-to-I approximation functions of Fig. 3(a) describe accurately the transconductor characteristic, when referring to their average values.

Let us now calculate the average normalized power of the three time-varying gain functions, viz., the square-wave power, $P_\square$, the triangular-wave power, $P_\triangledown$, and the power of the periodic function originating from the $tanh$ g_m-cell characteristic, P_{th}. With the aid of Parseval's theorem [12], these are calculated as given by (22)–(24)

$$P_\square = \frac{1}{T_2}\int_{-T_2/2}^{T_2/2} g_\square^2(t)dt = \frac{2}{T_2}\int_0^{\tau/2} g^2 dt = g^2 d = g\frac{I_{\rm TAIL}}{v_{S,B}} \tag{22}$$

$$\begin{aligned} P_\triangledown &= \frac{1}{T_2}\int_{-T_2/2}^{T_2/2} g_\triangledown^2(t)dt = \frac{2}{T_2}\int_0^{\tau} g^2\left(1-\frac{t}{\tau}\right)^2 dt \\ &= \frac{2}{3}g^2 d = \frac{2}{3}P_\square \end{aligned} \tag{23}$$

$$\begin{aligned} P_{th} &= \frac{1}{T_2}\int_{-T_2/2}^{T_2/2} g_{th}^2(t)dt = \frac{2}{\pi v_s}\int_0^{4V_T}\left(\frac{\partial i_{\rm OUT}(v)}{\partial v}\right)^2 dv \\ &= \frac{2g^2}{\pi v_s}\int_0^{4V_T}\frac{dv}{ch^4\frac{v}{2V_T}} \\ &= \frac{2g^2}{\pi v_s}\left[\frac{2}{3}V_T\frac{th\frac{v}{2V_T}}{ch^2\frac{v}{2V_T}} + \frac{4}{3}V_T th\frac{v}{2V_T}\right]_0^{4V_T} \\ &\cong 2.18\frac{2g^2}{\pi v_s}\frac{2}{3}V_T = \frac{2.18}{3}\frac{gI_{\rm TAIL}}{\pi v_s} = \frac{2.18}{3}P_\square \\ &\cong P_\triangledown. \end{aligned} \tag{24}$$

As suggested by the above results, the normalized power of the triangular description of the periodic gain function, (23), is almost identical to (24) that is obtained from the transconductor characteristic of (13). The square-wave approximation of the small-signal g_m-cell gain however overestimates the normalized power of the periodic gain function obtained from the $tanh$ characteristic of (13) by a factor close to 3/2.

The equality of the average values, (15) and (16), and the close proximity of the normalized power values, (23) and (24), of the triangular approximation of the small-signal g_m-cell gain and the actual g_m-cell gain qualifies the former gain function of the transconductor for the oscillator analysis. Therefore, we will refer to the triangular-wave g_m-cell gain as to the g_m-cell gain in this paper. Also, we will refer to the duty cycle d of the square-wave gain function as to the duty cycle of the g_m-cell gain function.

In the remainder of this section, we will first determine the Fourier coefficients of the triangular small-signal g_m-cell gain. Then, the harmonic components of the large-signal g_m-cell transfer function will be determined. The harmonic components of the corresponding gain functions are needed for the spectral noise analysis and calculation of the phase noise, as will be demonstrated in the following sections.

B. Complex Fourier Coefficients of the Time-Varying Small-Signal g_m-Cell Gain

The noise from the *LC*-tank and transistors Q_1 and Q_2 is modulated by the time-varying gain g_{IN}. Consequently, *noise folding* occurs, i.e., noise from a number of frequencies is converted into phase-noise at one frequency. In order to calculate the noise contributions of the g_m-cell and *LC*-tank to the resonator phase-modulating noise component (see Fig. 1)

using spectral analysis method, the spectrum of the small-signal g_m-cell gain (i.e., spectral magnitude components) shown in Fig. 3(b) has to be determined.

The magnitudes of the harmonic components of the complex Fourier development of the time-varying gain g_{IN} are given by (25) [12]

$$g_{2i} = gd\left(\frac{\sin(i\pi d)}{i\pi d}\right)^2. \tag{25}$$

Gain $g_{\rm IN}$ has harmonic components at even multiples of the oscillation frequency only (multiples of $2f_0$). For the sake of simplicity, all coefficients are used positive (as magnitudes) in the spectral representations, as suggested by definitions (1), (2).

For $k \gg 1$ and with the aid of (20), (25) simplifies to

$$g_{2i} = gd = \frac{g_m}{2}d \tag{26}$$

for the components up to around a first zero-crossing frequency of the envelope sinc function of (25) (i.e., for $id < 1, i = 0, 1, 2, \ldots$). For higher frequencies, the magnitudes of the harmonic components reduce according to (25).

C. Complex Fourier Coefficients of the g_m-Cell Switching Function

The noise of the bias current source is switched between each half of the *LC*-tank (± 1 squarewave function) by the f_0-periodic transconductor limiting characteristic, shown in Fig. 3(c). This results in folding of the bias current source noise.

The complex Fourier coefficients of the square-wave switch function are positioned at odd multiples of the oscillation frequency. Their magnitudes (thus positive real numbers) are defined by (27) for $k \gg 1$

$$c_{2i+1} = \left|\frac{\sin\left((2i+1)\pi/2\right)}{(2i+1)\pi/2}\right|. \tag{27}$$

IV. Phase-Noise Model of Bipolar *LC*-Oscillators

For the bipolar *LC*-oscillator shown in Fig. 2 and its model in Fig. 1(a), we consider the case where the g_m-cell operates for a large portion of the oscillation period in the limiting region, provided a large voltage swing and small-signal loop gain. This is a typical region of operation for high-performance oscillators [15].

The noise from the *LC*-tank and transistors Q_1 and Q_2 (both contributions) is modulated by the small-signal time-varying g_m-cell gain. It is converted from around a number of multiples of the oscillation frequency into the phase-noise at one frequency. In a similar manner, the noise of the bias current source is periodically switched to the *LC*-tank via transistors Q_1 and Q_2 resulting in folding of the bias current source noise from around a number of f_0 multiples into the phase noise at around f_0.

In the following subsections, we derive a closed-form expression for the phase noise of switching bipolar *LC* oscillators, analyzing the oscillator noise performance in the *spectral* domain. After determining the oscillation condition, we evaluate for each of the noise sources (*LC*-tank, g_m-cell, and bias current source noise):

(a) the double-sided folded noise components at $\pm f_0 \pm \Delta$;
(b) the single-sided phase-modulating noise component at $f_0 + \Delta$;
(c) the phase-related noise power;
(d) the transfer function to the resonator.

Finally, we determine the phase noise of the oscillator from (a)–(d). The results obtained for bipolar oscillators are general and can be used to derive the phase-noise model of CMOS *LC*-oscillators.

A. Oscillation Condition

The amplitude of the fundamental current at the output of the g_m-cell is obtained by multiplying the oscillation signal voltage components $(v_{S,B}/2)$ by the g_m-cell harmonics: $v_{S,B}/2$ at $+f_0$/-f_0 is multiplied by g_0 and g_{-2}/g_2 and shifted to $-f_0/+f_0$. After transformation to positive frequencies, the obtained current amplitude is converted into voltage at the output of the resonator by its impedance at resonance R_{TK}, (28)

$$\left(\frac{v_{S,B}(-f_0)}{2}g_0 + \frac{v_{S,B}(+f_0)}{2}g_0 + \frac{v_{S,B}(-f_0)}{2}g_2 + \frac{v_{S,B}(+f_0)}{2}g_{-2}\right)R_{TK} = (g_0+g_2)v_{S,B}R_{TK}. \tag{28}$$

As the signal amplitudes at the input of the g_m-cell and the output of a divider proceeding the resonator are equal in steady state, the oscillation condition for the switching oscillators can be derived from (28) as

$$g_0 + g_2 = nG_{TK} \tag{29}$$

or with the aid of (25) as

$$gd\left(1 + \left(\frac{\sin(\pi d)}{\pi d}\right)^2\right) \cong 2gd = g_m d = nG_{TK}. \tag{30}$$

The duty cycle d determined from (30) results in (20), as expected. The product gd equals $nG_{TK}/2$, being the average value of the g_m-cell time-varying gain functions given by (14)–(16).

B. LC-Tank Noise

Harmonic components of the *band-limited* *LC*-tank noise (v_N) at input of the g_m-cell (i.e., output of the divider) at $\pm f_0 \pm \Delta$ and harmonic components g_0 and $g_{\pm 2}$ of the time-varying small-signal g_m-cell gain are shown in Fig. 4, together with spectral representations of the convolution (i.e., multiplication and shifting in the frequency domain) between these harmonic components.

(a) After convolution, the *LC*-tank noise current components at the output of the g_m-cell at $\pm f_0 \pm \Delta$ are given by (31) and (32), as shown in Fig. 4

$$i_{N,O}(f_0 \pm \Delta) = g_0 v_N(f_0 \pm \Delta) + g_2 v_N(-f_0 \pm \Delta) \tag{31}$$

$$i_{N,O}(-f_0 \pm \Delta) = g_0 v_N(-f_0 \pm \Delta) + g_{-2} v_N(f_0 \pm \Delta). \tag{32}$$

(b) The phase-modulating noise component (single-sided) i_{PM} at frequency $f_0+\Delta$ is obtained by combining the current noise contributions $i_{N,O}$ at $\pm f_0 \pm \Delta$ as implied by the generic phase noise model and (1)–(3)

$$i_{PM}(f_0+\Delta)=\frac{1}{2}i_{N,O}(f_0+\Delta)+\frac{1}{2}i_{N,O}(-f_0+\Delta) +\frac{1}{2}i_{N,O}(-f_0-\Delta)+\frac{1}{2}i_{N,O}(f_0-\Delta). \quad (33)$$

After summing the currents of the correlated noise components ($g_{\pm 2i}v_N(f_0+\Delta)$ correlated with $g_{\pm 2i}v_N(-f_0-\Delta)$ and $g_{\pm 2i}v_N(f_0-\Delta)$ correlated with $g_{\pm 2i}v_N(-f_0+\Delta)$) as

$$i_{PM}(f_0+\Delta)=(g_0+g_2)v_N(f_0+\Delta)+(g_0+g_2)v_N(f_0-\Delta) \quad (34)$$

the phase-related noise power at $f_0+\Delta$ is calculated

$$i^2_{PM}(f_0+\Delta)=\frac{1}{2}\left[(g_0+g_2)^2v^2_N(f_0+\Delta) +(g_0+g_2)^2v^2_N(f_0-\Delta)\right] \quad (35)$$

where the factor 1/2 relates to rms power.

(c) As the magnitudes of the harmonic components of the *LC*-tank white noise at input of the transconductor are equal ($v^2_N(R_{TK})=v^2_N(f_0\pm\Delta)$), (35) reduces to

$$i^2_{PM}(R_{TK})=(g_0+g_2)^2\frac{v^2_N(R_{TK})}{n^2}. \quad (36)$$

(d) The gain from the double-sided *LC*-tank voltage noise density $v^2_N(R_{TK})=2KTR_{TK}$ back to the *LC*-tank current-noise density (via the divider and g_m-cell) is obtained from (36) as

$$g^2(R_{TK})=\frac{(g_0+g_2)^2}{n^2}. \quad (37)$$

With the aid of (4) and (29), the contribution of the *LC*-tank noise to the phase noise, prior to shaping by the *LC*-tank impedance $Z(\Delta\omega)$, equals

$$\mathcal{L}(R_{TK})=\frac{i^2_{PM}(R_{TK})}{v^2_S/2}=\frac{2(g_0+g_2)^2v^2_N(R_{TK})}{n^2v^2_S} =\frac{2G^2_{TK}v^2_N(R_{TK})}{v^2_S}=\frac{4KTG_{TK}}{v^2_S}. \quad (38)$$

If we relate the contribution of each noise source ns (prior to shaping by the *LC*-tank band-pass characteristic) to phase noise $\mathcal{L}(ns)$ by a noise factor $F(ns)\triangleq v^2_S\mathcal{L}(ns)/(4KTG_{TK})$, we obtain the *LC*-tank noise factor $F(R_{TK})$ from (38) as

$$F(R_{TK})=\frac{v^2_S\mathcal{L}(R_{TK})}{4KTG_{TK}}=1. \quad (39)$$

The contributions of other oscillator noise source to phase noise can be conveniently compared to the contribution of the *LC*-tank by referring to its noise factor of one.

C. Base-Resistance Thermal Noise

The base-resistance thermal noise $v_N(r_B)$ at $\pm(2i+1)f_0\pm\Delta$ fold to the resonator via the harmonic components $g_{\pm 2i}$, given the small-signal time-varying gain shown in Fig. 3(b). The maximum gain is $g=g_m/2$ in the linear and zero in the g_m-cell limiting region, suggesting that $v_N(r_B)$ does not contribute to the phase-noise in the limiting region.

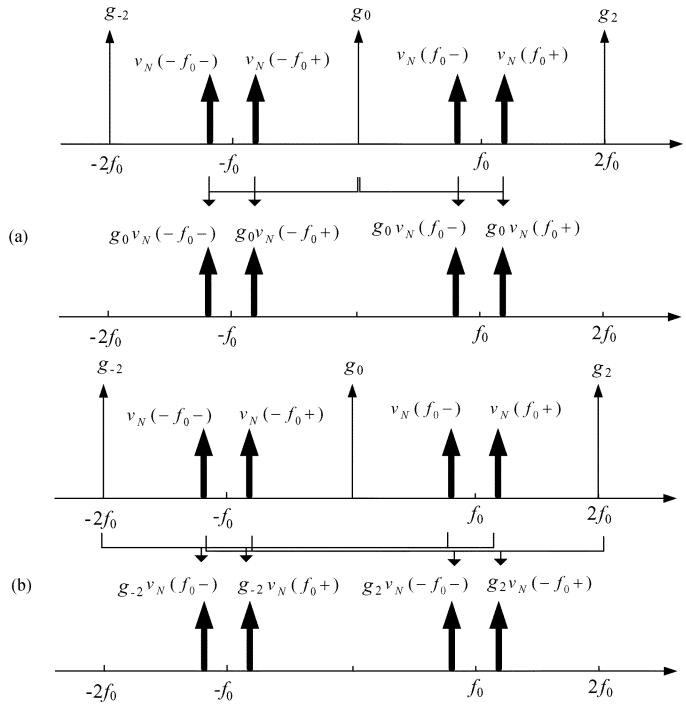

Fig. 4. Result of the convolution between (a) g_0 harmonic and *LC*-tank noise, (b) $g_{\pm 2}$ harmonics and *LC*-tank noise.

(a)–(b) Harmonic components of the base-resistance noise at $\pm f_0\pm\Delta$ convolve in the same wave as the *LC*-tank noise at these frequencies, which is shown in Fig. 4(a) and (b). Unlike the band-limited *LC*-tank noise, the g_m-cell noise folds back to the resonator around the oscillation frequency from around all *odd* harmonic components.

Assuming all base-resistance noise components undergo the same transformation mechanism, the convolution of the noise components at $\pm f_0\pm\Delta$, $\pm 3f_0\pm\Delta$, $\pm(2i+1)f_0\pm\Delta$ with $g_0, g_{\pm 2},\ldots,g_{\pm 2i}$ results in a PM noise component at $f_0+\Delta$, which is obtained by generalizing (34) as

$$\begin{aligned} i_{PM}(f_0+\Delta)=&(g_0+g_2)v_N(f_0+\Delta)\\ &+(g_0+g_2)v_N(f_0-\Delta)\\ &+(g_2+g_4)v_N(3f_0+\Delta)\\ &+(g_2+g_4)v_N(3f_0-\Delta)+\ldots\\ &+(g_{2i-2}+g_{2i})v_N\left((2i-1)f_0+\Delta\right)\\ &+(g_{2i-2}+g_{2i})v_N\left((2i-1)f_0-\Delta\right). \end{aligned} \quad (40)$$

For example, noise components at $\pm 3f_0\pm\Delta$ convolve with $g_{\pm 2}$ and $g_{\pm 4}$, resulting in the contribution shown in the third and fourth rows of (40).

(c) As the magnitudes of the harmonic components of the white base-resistance noise are equal, the phase-related noise power at $f_0+\Delta$ is obtained from (40) as

$$i^2_{PM}(r_B)\left[(g_0+g_2)^2+(g_2+g_4)^2+\ldots +(g_{2i-2}+g_{2i})^2\right]v^2_N(r_B). \quad (41)$$

Assuming equality of the neighboring coefficients g_{2i}, and by replacing $2g_{2i-2}g_{2i}$ by $g_{2i-2}^2+g_{2i}^2$ subsequently, the above summation becomes

$$\begin{aligned} i_{PM}^2(r_B) &= \left[2g_0^2+4g_2^2+4g_4^2+\ldots+4g_{2i-2}^2+\ldots\right] v_N^2(r_B) \\ &= 2\left(g_0^2+2\sum_{i=1}^{\infty}|g_{2i}|^2\right) v_N^2(r_B) \\ &= v_N^2(r_B)\frac{1}{T_2}\int_{-T_2/2}^{T_2/2} g_{\nabla}^2(t)dt. \end{aligned} \tag{42}$$

The summation obtained can be determined employing the Parseval's theorem, by relating this summation power series to (23) [12]. The phase-related noise power of the base-resistance g_m-cell noise at $f_0+\Delta$ is now obtained from (22), (23), and (42). This is given by (43)

$$i_{PM}^2(r_B) = \frac{4}{3}g^2 d v_N^2(r_B). \tag{43}$$

Note that in the above analysis infinite bandwidth of operation of the transconductor devices and their noise sources have been implicitly assumed. Therefore, (43) is the worst-case noise contribution of the g_m-cell base-resistance noise. Namely, the summation of (42) is limited by the finite bandwidth of the g_m-cell devices and corresponding noise source. If the bandwidth were limited to a value f_B, the number of the folding components in (42) would be $f_B/(2f_0)$. For example, if f_B is the zero crossing of the sinc envelope function of (25), the number of the folding components is $2f_0/(2f_0d)=2k$ [see Fig. 3(b)]. We will return to this point later.

(d) The gain from the double-sided base-resistance voltage noise density $v_N^2(r_B)$ to the *LC*-tank as current-noise density, via the g_m-cell, is now derived from (43) as

$$g^2(r_B) = \frac{4}{3}dg^2 = \frac{4}{3}d\left(\frac{g_m}{2}\right)^2 = \frac{4}{3}\frac{1}{2k}(nkG_{TK})^2 = \frac{2}{3}kn^2G_{TK}^2. \tag{44}$$

The gain from the base-resistance noise is a function of the duty cycle d and the maximum of the small-signal g_m-cell gain g as well as a function of the small-signal loop gain k, divider ratio n, and *LC*-tank conductance G_{TK}.

The contribution of the $v_N(r_B)$ to the phase noise can be now calculated from (43) and (44). This is given by (45)

$$\begin{aligned} \mathcal{L}(r_B) &= \frac{i_{PM}^2(r_B)}{v_S^2/2} = \frac{4kn^2G_{TK}^2v_N^2(r_B)}{3v_S^2} \\ &= \frac{4kn^2G_{TK}^2 2KTr_B}{3v_S^2} = \frac{8KTG_{TK}nr_BG_{TK}nk}{3v_S^2}. \end{aligned} \tag{45}$$

Taking into account both transistors of the g_m-cell, the total base-resistance phase-noise contribution is twice that of (45), resulting in a noise factor $F(2r_B)$, (46)

$$\begin{aligned} F(2r_B) &= \frac{v_S^2\mathcal{L}(2r_B)}{4KTG_{TK}} = \frac{8KTG_{TK}nr_BG_{TK}2nk}{12KTG_{TK}} \\ &= \frac{4}{3}nknr_BG_{TK} = \frac{2}{3}nkc. \end{aligned} \tag{46}$$

where $c=r_B2nG_{TK}$ is a start-up constant.

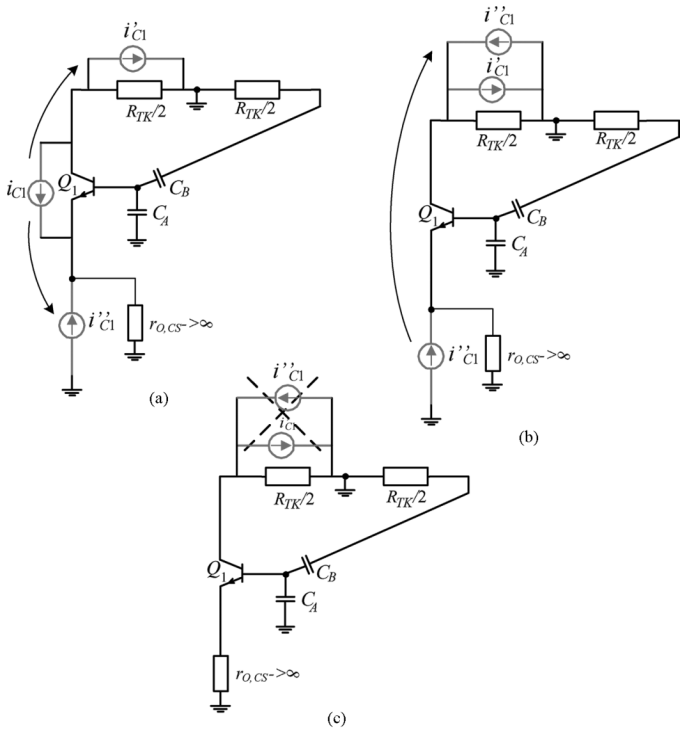

Fig. 5. Splitting of the collector-current shot noise in the g_m-cell limiting region.

This result suggests that the contribution of the g_m-cell base-resistance noise to the phase noise of the oscillator under consideration is directly proportional to the small-signal loop gain k (and thus to the power consumption) and parameters n and c, the latter relating r_B of the transconductor transistors and the quality of the resonator.

D. Transconductor Shot Noise

The contribution of the transconductor shot noise to the PM noise component at the resonator can be determined following the procedure outlined in the previous section. As collector-current and base-current shot noise sources are already at input and output of the resonator, respectively, their phase-noise contributions can be determined by taking into account the effect of the noise modulation due to the switching of the transconductor. Even though the g_m-cell base-current shot noise contributes to the *LC*-tank phase-modulating component at all times, it is around an order of magnitude smaller than the collector-current shot noise [see (11)] as well as its contribution to the phase noise. We will therefore consider the collector-current shot noise only in the remainder of this section. However, a special care has to be taken in the design of the g_m-cell base-bias circuitry, as otherwise the contribution of the base-current shot noise may be enhanced (e.g., for a low-impedance of the g_m-cell base biasing circuit).

When only Q_1 (or Q_2) is active, $i_N(I_C)$ does not flow to the resonator, due to the large impedance at the emitter of the g_m-cell transistor. This is expected, considering Q_1 as a common-base like transistor in this case. The situation where only Q_1 is active is described in Fig. 5(a): the collector-emitter oriented noise source i_C is split into the collector-to-ground

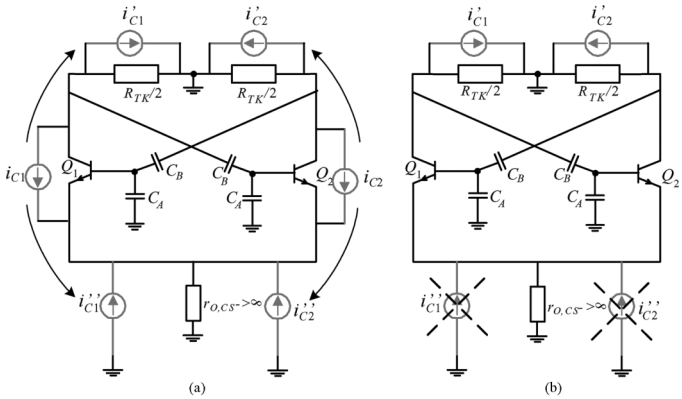

Fig. 6. Transformation of the collector-current shot-noise sources in the g_m-cell linear region.

and ground-to-emitter oriented sources, i'_C and i''_C, respectively. After i''_C is referred from emitter to collector of the common-base-like transistor Q_1, thus with a gain of around one [see Fig. 5(b)], the noise sources i'_C and i''_C cancel at the resonator, Fig. 5(c).

The transconductor collector-current shot noise contributes to the PM noise component at the resonator when Q_1 and Q_2 are simultaneously active. We will first determine the contribution of $i_N(I_C)$ to the *LC*-tank in the linear region of the transconductor using circuit analysis, and then consider the modulation of the transconductance by referring to the g_m-cell small-signal time-varying transfer function.

Each current noise source can be split as shown in Fig. 6(a): the collector-emitter oriented noise sources i_C are split into the collector-to-ground and ground-to-emitter oriented sources, i'_C and i''_C, respectively (indices 1 and 2 refer to Q_1 and Q_2 in Fig. 6). Whereas the common-mode sources i''_C can be neglected, the sources i'_C appear across a half the tank resistance $1/2R_{TK}$ each [see Fig. 6(b)], generating the single-sided PM noise voltage component as given by (47). Here, we have assumed that noise i_C adds completely to the phase noise (with single-sided noise current density $2i_N^2(I_C)$)

$$v_{PM}'^2(I_C) = \frac{2i_N^2(I_C)R_{TK}^2}{4}. \tag{47}$$

The total contribution of each collector-current shot-noise source in the g_m-cell *linear* region to the phase-modulating noise current component, referred to the complete *LC*-tank R_{TK}, equals

$$i_{PM}'^2(I_C) = \frac{v_{PM}'^2(I_C)}{R_{TK}^2} = \frac{i_N^2(I_C)}{2} = KT\frac{g_m}{2}. \tag{48}$$

This shows that the total gain from the g_m-cell collector-current shot noise sources to the *LC*-tank equals 1/2 [compare (11) and (48)], when both g_m-cell transistors are simultaneously active.

(a–c) The *LC*-tank referred power of the g_m-cell shot noise $KTg_m/2$ is modulated by the switching function of the g_m-cell, that is, by the function g_{IN} of Fig. 3(b), however with a gain g of 1. The total power of the phase-modulating noise component at $f_0 + \Delta$ originating from each g_m-cell collector-current shot noise source, is obtained by averaging the transistor transconductance (and noise density of (48), accordingly) over a period of oscillation. Calculating the average of the time-varying noise modulating function (Fig. 3(b) with $g = 1$) from (15) as d, $i_{PM}^2(I_C)$ becomes

$$i_{PM}^2(I_C) = d\frac{i_N^2(I_C)}{2}. \tag{49}$$

(d) The gain from the double-sided collector-current shot-noise to the PM noise component referred to the *LC*-tank now equals

$$g^2(I_C) = \frac{d}{2} = \frac{1}{4k} \tag{50}$$

being inversely proportional to the small-signal loop gain.

The contribution of the $i_N(I_C)$ to the phase noise becomes

$$\begin{aligned}\mathcal{L}(I_C) &= \frac{i_{PM}^2(I_C)}{v_S^2/2} = \frac{2}{4k}\frac{i_N^2(I_C)}{v_S^2} = \frac{2}{4k}\frac{2KTg_m/2}{v_S^2} \\ &= \frac{KTG_{TK}n}{v_S^2}.\end{aligned} \tag{51}$$

Taking into account the contributions of the collector-current shot-noise sources from both transconductor transistors, a noise factor $F(2I_C)$ is obtained as given by (52)

$$F(2I_C) = \frac{v_S^2\mathcal{L}(2I_C)}{4KTG_{TK}} = \frac{2KTG_{TK}n}{4KTG_{TK}} = \frac{n}{2}. \tag{52}$$

Equation (52) suggests that the phase-noise contribution of the g_m-cell collector-current shot-noise is independent of the small-signal loop gain and power consumption, but proportional to the capacitive divider ratio n, for $k \gg 1$.

E. Bias Current Source Noise

Folding of the bias current source (BCS) noise is a result of the operation of the g_m-cell in the limiting region. Having the harmonic components at odd multiples of the oscillation frequency, $c_{\pm(2i+1)}$, given by (27), the g_m-cell switching function [see Fig. 3(c)] converts the BCS noise components at around even multiples of the oscillation frequency back to the *LC*-tank at around the oscillation frequency. Note that we refer to the magnitudes of the Fourier components of the transconductor switching characteristic, thus, positive real numbers. This is done in order to comply with the definition of the phase noise given by Fig. 1(b) and (1)–(4).

For the sake of simplicity, we will first consider the convolution between the harmonic components $c_{\pm1/\pm3}$ at $\pm f_0$ and $\pm 3f_0$ with the BCS noise components at $\pm\Delta$ and $\pm 2f_0 \pm \Delta$. Then, we will derive an expression for the contribution of the BCS noise to the phase noise, by generalizing this result for all harmonic products.

(a) The convolution of the BCS noise $i_N(I_{BCS})$ at $\pm\Delta$, $\pm 2f_0 \pm \Delta$ with harmonics $c_{\pm1}$ results in a *differential* noise component $i_{N,O}$, referred to the output of the transconductor at $\pm f_0 \pm \Delta$, that is given as follows:

$$i_{N,O}(f_0 \pm \Delta) = c_{-1}i_N(2f_0 \pm \Delta) + c_1 i_N(\pm\Delta) \tag{53}$$

$$i_{N,O}(-f_0 \pm \Delta) = c_{-1}i_N(\pm\Delta) + c_1 i_N(-2f_0 \pm \Delta). \tag{54}$$

Similarly, a convolution of the noise $i_N(I_{BCS})$ at $\pm 2f_0 \pm \Delta$ and $\pm 4f_0 \pm \Delta$ with harmonics $c_{\pm 3}$ results in

$$i_{N,O}(f_0 \pm \Delta) = c_{-3} i_N(4f_0 \pm \Delta) + c_3 i_N(-2f_0 \pm \Delta) \quad (55)$$
$$i_{N,O}(-f_0 \pm \Delta) = c_{-3} i_N(2f_0 \pm \Delta) + c_3 i_N(-4f_0 \pm \Delta). \quad (56)$$

(b) A differential phase-modulating noise component (single-sided spectrum) at a frequency $f_0 + \Delta$ is obtained by combining the current noise contributions $i_{N,O}$ at $\pm f_0 \pm \Delta$ as given by (1), (2). The noise components at frequencies $\pm\Delta$ (i.e., $i_N(\pm\Delta)$) contribute purely to an AM component at $f_0 \pm \Delta$ [6], [16], [17]. Nonetheless, the noise components at $\pm\Delta$ (e.g., $1/f$ noise) can be converted to a frequency-modulating (FM) component, via AM-to-FM conversion mechanism of the *LC*-tank varactor, which can't be distinguished from PM components [16], [17]. However, as this is beyond the scope of this paper, we will proceed our analysis accounting for PM-contributing components only. Doing so, (53)–(56) yield (57) (BCS noise at $\pm\Delta$ and $\pm 2f_0 \pm \Delta$ considered)

$$i_{PM,\mathrm{DIFF}}(f_0 + \Delta) = (c_1 + c_3) i_N(2f_0 + \Delta) + (c_1 + c_3) i_N(2f_0 - \Delta) + \ldots. \quad (57)$$

(c) From (57), a general rule can be found for the convolution between the harmonics of the BCS noise and the transconductor switching characteristic of Fig. 3(c). Assuming the equalities $c_{(2i+1)} = c_{-(2i+1)}$, and $i_N(\pm\Delta) = i_N(\pm 2f_0 \pm \Delta) = i_N((\pm 2i+1)f_0 \pm \Delta) = i_N(I_{BCS})$, a complete formula for the differential phase-related power of the BCS noise referred to the *LC*-tank is given by (58)

$$i^2_{PM,\mathrm{DIFF}}(I_{BCS}) = \left((c_1 + c_3)^2 + (c_3 + c_5)^2 + \ldots + (c_{2i-1} + c_{2i+1})^2\right) i^2_N(I_{BCS}). \quad (58)$$

Using the weights of a 50% duty cycle square-wave [12], the summation series of (58) can be calculated as $i^2_{PM,\mathrm{DIFF}}(I_{BCS}) = i^2_N(I_{BCS})$. As the current through the *LC*-tank is one half the differential current component, the phase-related noise power (related to the resonator as a whole) equals

$$i^2_{PM}(I_{BCS}) = \frac{i^2_{PM,\mathrm{DIFF}}(I_{BCS})}{4} = \frac{i^2_N(I_{BCS})}{4}. \quad (59)$$

(d) The transfer function from the double-sided bias current noise density $i^2_N(I_{BCS})$ to the *LC*-tank is now derived from (59) as $g^2(I_{BCS}) = 1/4$.

The contribution of the bias current source noise to the phase noise is obtained as

$$\mathcal{L}(I_{BCS}) = \frac{i^2_{PM}(I_{BCS})}{v_S^2/2} = \frac{i^2_N(I_{BCS})}{2v_S^2} = \frac{KTg_m(1 + 2r_B g_m)}{v_S^2} \quad (60)$$

where we have used $g_{m,CS} = 2g_m$ and assumed $2r_{B,CS} = r_B$, given approximately the same transit frequencies (f_T) of transistors Q_1, Q_2, and Q_{CS} (thus, Q_{CS} twice as large as Q_1, Q_2 is assumed).

Finally, a noise factor $F(I_{BCS})$ results, as given by (61)

$$F(I_{BCS}) = \frac{2i^2_{PM}(I_{BCS})}{4KTG_{TK}} = \frac{KTg_m(1 + 2r_B g_m)}{4KTG_{TK}} = \frac{KT2knG_{TK}(1 + 2kc)}{4KTG_{TK}} = k\left(\frac{n}{2} + nkc\right). \quad (61)$$

For transistor Q_{CS} (see Fig. 2) of arbitrary dimensions, and $\alpha r_{B,CS} = r_B$ (Q_{CS} larger than Q_1, Q_2 for $\alpha > 1$, and smaller for $\alpha < 1$, α being a ratio of the areas of Q_{CS} and Q_1, Q_2), a general formulation of (61) reads

$$F(I_{BCS}) = F(I_{C,CS}) + F(r_{B,CS}) = k\left(\frac{n}{2} + 2nkc/\alpha\right) \quad (62)$$

where $F(I_{C,CS})$ and $F(r_{B,CS})$ stand for the noise factors of the bias current source collector-current shot noise and base-resistance thermal noise, respectively.

Comparing the result obtained with the noise factors of the g_m-cell collector-current shot noise and base-resistance thermal noise sources, (46) and (52), (62) becomes

$$F(I_{BCS}) = k\left(F(2I_C) + 3F(2r_B)/\alpha\right). \quad (63)$$

We observe from (63) that the contribution of the bias current source noise to the phase noise of the *LC*-oscillator under consideration is larger than all other contributions together [9]. In particular, the contribution of the BCS is a factor of around k larger than the contribution of the g_m-cell for $\alpha \sim 3$. For a typical small-signal loop gain of around 10, this would result in an unacceptable degradation of the phase noise of around 10 dB from the calculations. Finally, it is important to note that (61) holds for $k \gg 1$, thus for the hard switching of the transconductor. At $k = 1$, the contribution from the BCS noise is small, being a common-mode signal. Without loss of generality, and for a convenient formulation, we will use (61) in the remainder of this paper unless stated otherwise.

Finally, note that the result obtained assumes infinitely large bandwidth of the operation of the bias current source devices and their noise sources. Equation (61) therefore overestimates the contribution of the BCS noise to the phase noise, as the operational bandwidth of the devices and their noise sources is limited. Moreover, the g_m-cell switching function deviates from a perfect square-wave [see Fig. 3(c)], thereby reducing the contribution of the BCS noise additionally. We will come to this point soon.

F. Noise Factor and Phase Noise for Bipolar LC-Oscillators

Assumed to be uncorrelated, all noise sources, viz., the tank conductance noise, the base resistance noise, the transconductor shot noise, and the bias current noise, add up to an equivalent phase-modulating noise component at the resonator. With the aid of (39), (46), (52), and (61), the noise factor of the bipolar *LC* oscillator now reads as given by (64) and (65)

$$F = F(R_{TK}) + F(2I_C) + F(2r_B) + F(I_{BCS}) \quad (64)$$
$$F = 1 + (1 + k)\frac{n}{2} + \left(\frac{2}{3} + k\right) nkc. \quad (65)$$

The phase noise at an offset frequency Δ from the oscillation frequency f_0 is determined with the aid of (5) as

$$\mathcal{L} = \frac{2i_{PM,\mathrm{TOT}}^2}{v_S^2(4\pi C_{\mathrm{TOT}}\Delta)^2} = \frac{4KTG_{TK}F}{v_S^2(4\pi C_{\mathrm{TOT}}\Delta)^2} = \frac{\mathcal{L}(R_{TK}) + \mathcal{L}(2I_C) + \mathcal{L}(2r_B) + \mathcal{L}(I_{BCS})}{(4\pi C_{\mathrm{TOT}}\Delta)^2} \quad (66)$$

where C_{TOT} stands for the *LC*-tank total capacitance. Substituting (18) into (66), the phase noise finally becomes

$$\mathcal{L} = \frac{4KTG_{TK}}{(4\pi C_{\mathrm{TOT}}\Delta)^2}\left(\frac{\pi}{8V_T}\right)^2 \frac{1 + (1+k)\frac{n}{2} + \left(\frac{2}{3}+k\right)nkc}{k^2n^2}. \quad (67)$$

The result obtained is a comprehensive description of the phase-noise phenomenon in the *LC* oscillator under consideration. The developed model does not require use of numerical solvers, yet providing oscillator designers with a valuable tool for analysis and synthesis of high-performance oscillators. The phase-noise model of (67) is valid as long as voltage swing and phase noise improve with current consumption (and k). Conditions for the maximum voltage swing and small-signal loop gain can be found in [15].

It is important to note that (65) gives the worst-case noise factor of the bipolar oscillator under consideration, thereby overestimating its phase noise by using (67). The small-signal loop-gain related contributions, viz., the base-resistance noise contribution of the transconductor, (46), and the base-resistance and collector-current noise contributions of the bias current source, (61), are calculated implicitly assuming infinite operational bandwidth of both the noise sources and the oscillator devices. However, the limited operation bandwidth of the devices and noise sources of the transconductor and bias current source alleviate the effect of the noise folding: the noise power around higher harmonic components is small as are the corresponding devices gain parameters, as expected. Moreover, a finite transconductor switching time (thus not an ideal square-wave function) additionally ameliorates the BCS noise contribution. The exact small-signal loop-gain dependent contributions are therefore smaller than (46) and (61). It is expected that low-power, low-frequency, large loop-gain oscillators with high f_T of the devices available approach the results of the calculations: the lower the oscillation frequency, the more noise components fold within the operational bandwidth; the faster the switching of the g_m-cell, the more BCS noise components fold to the resonator. Deviations of the calculated phase-noise contributions from those of a "real" oscillator design can be estimated using oscillator simulators accounting for the bandwidth limitations. Next sections detail on this.

However, the results obtained are intuitive and describe qualitatively the complex phase-noise generating mechanisms in *LC*-oscillators. The formulations derived are amenable for making qualitative and quantitative design decisions as they describe the oscillator phase-noise performance using electrical parameters.

G. Bipolar LC-Oscillator With Directly Coupled LC-Tank and g_m-Cell

Bipolar *LC*-oscillators are often designed with their *LC*-tank directly coupled to the active part, that is, the oscillator of Fig. 2 with a short between the bases and corresponding collectors of Q_1, Q_2 ($V_B = V_{CC}$), or with $C_A = 0$ and $C_B = \propto$. Such an oscillator is just a special case of the oscillator of Fig. 3, with a capacitive divider ratio $n = 1$.

The phase-noise model derived for the directly coupled bipolar *LC*-oscillator is readily obtained from the model derived in the previous sections by substituting $n = 1$ in (65) and (67). This is given by (68) and (69)

$$F = 1 + \frac{1+k}{2} + \left(\frac{2}{3}+k\right)kc \quad (68)$$

$$\mathcal{L} = \frac{4KTG_{TK}}{(4\pi C_{\mathrm{TOT}}\Delta)^2}\left(\frac{\pi}{8V_T}\right)^2 \frac{1 + \frac{1+k}{2} + \left(\frac{2}{3}+k\right)kc}{k^2}. \quad (69)$$

An *LC* oscillator with $n = 1$ is a low-power counterpart of an oscillator with $n > 1$. A larger effective conductance of the g_m-cell seen by the *LC*-tank $(g_m/2)$ compensates the loss *LC*-tank conductance for lower bias current (I_{TAIL} in Fig. 2). The oscillator phase-noise analysis described in previous sections applies to directly coupled oscillators as well.

As CMOS *LC* oscillators are designed with a directly coupled *LC*-tank and active part, we can conveniently use the above formulations for performance comparison between the bipolar and CMOS *LC*-oscillators (as well as derivation of the phase-noise model for CMOS *LC*-oscillators [16]–[20]).

H. Implications of the Phase-Noise Model on Designs of Bipolar LC-Oscillator

In this section we will discuss the implications of the results obtained from the spectral noise analysis on the synthesis of bipolar *LC*-oscillators.

The contribution of the *LC*-tank noise to the phase noise is a constant (*LC*-tank noise factor $\sim$1), as is the contribution of the g_m-cell shot noise ($\sim 1/2n$). The phase-noise contribution of the g_m-cell base-resistance noise could surpass the contributions of the *LC*-tank noise and g_m-cell shot noise, given the operating small-signal loop gain (k) as well as the *LC*-tank designed and the g_m-cell transistors base resistance (factor c). This contribution is larger for a larger k. But, the voltage swing increases with k as well, resulting in a better net phase noise. All these contributions are however minor compared to the phase-noise contribution of the bias current source.

To better understand design implications of the phase-noise model derived let us consider three relevant design cases. Closer inspection of (67) reveals that for a large c ($\sim$1, thus, a large *LC*-tank conductance), and $k \sim 1$, the phase noise would be proportional to a constant c. For a large c and $k \gg 1$, the phase noise would improve with a small-signal loop gain k. On the other hand, for a low c ($\sim$0.01, thus, a high quality *LC*-tank), $k \gg 1$, and suppressed bias current-source noise [9], the phase noise would be proportional to $1/k^2$. Comparing the former with the latter two designs (the former is a design with a low quality *LC*-tank, unsuppressed BCS noise, and a small k, the second is a design with a low quality *LC*-tank, unsuppressed BCS noise, and

a large k, while the latter is a design with a high quality *LC*-tank, suppressed BCS noise, and large k), a factor of k and k^2 better phase noise results, respectively. In other words, for a typical value of $k \sim 10$, a factor $\sim$100 (or $\sim$20 dB) and $\sim$10 difference between low- and high-performance designs may result. These observations, derived from the phase-noise model obtained, are valuable to oscillator designers to make proper decisions in an early design phase.

V. Verification of Phase-Noise Model for Bipolar *LC*-Oscillators

The phase-noise model obtained from the spectral analysis of noise in *LC*-oscillators is verified in this section by comparing the theoretical calculation results of the phase-noise model for a bipolar *LC*-oscillator with the results obtained from the simulations. Other phase-noise analysis methods for bipolar *LC*-oscillators found in literature are also discussed in this section.

A. Results of Simulations for the Bipolar LC-Oscillator

In this section, calculation and simulation results for the bipolar oscillator shown in Fig. 2 are compared in terms of noise factors, $F(2I_C)$, $F(2r_B)$, $F(r_{B,CS})$, $F(I_{C,CS})$ (the latter two being the noise factors of the base-resistance thermal noise and collector-current shot noise of a bias current source transistor). The noise factors simulated are determined relative to the phase-noise contribution of the *LC*-tank, $F(R_{TK}) = 1$. The oscillator shown in Fig. 2 is simulated using SpectreRF with the following parameters (extracted from the layout [9]): oscillation frequency $f_0 \sim 5.74$ GHz, tank resistance $R_{TK} \sim 340\ \Omega$, capacitive divider ratio $n \sim 1.6$, start-up constant $c \sim 0.25$, supply voltage $V_{CC=}2.2$ V. Emitter area of the bias current source transistors is twice that of the g_m-cell transistors.

For fair comparison of the simulation and calculation results, the simulated circuit parameters have been used in the calculations. In particular, a good estimation of the small-signal loop gain k is needed, as it is a corner-stone parameter of the phase-noise model.

The small-signal loop gain k equals $R_{TK}g_{m-CA}/(2n)$, where $g_{m-CA}/(2n)$ stands for the calculated transconductance of the g_m-cell that is seen by the *LC*-tank. However, the effective transconductance of the cross-coupled g_m-cell seen by the *LC*-tank, $g_{m-EF}/(2n)$, which is determined from the simulations, is smaller than $g_{m-CA}/(2n)$. The most apparent reason is the feedback effect of the transistors' emitter resistors reducing the transconductance. A relationship between the small-signal loop gain k used in the phase-noise formulations and the effective small-signal loop-gain k_{EF} ($k > k_{EF}$) obtained from the simulations is given by (70)

$$k = g_{m-CA}\frac{R_{TK}}{2n} > g_{m-EF}\frac{R_{TK}}{2n} = k_{EF}. \qquad (70)$$

A factor of around 1.5 between the two loop-gain values (k and k_{EF}) has been estimated from the simulation for $k \gg 1$. Results of simulations and calculations (obtained by replacing k with k_{EFF} in the corresponding formulae) are compared for the same effective k, and then referred to the small-signal loop gain k used in the phase-noise derivations. Four distinct k values larger than one have been considered: 4, 6, 8, and 9.6, the latter providing the best phase-noise simulated.

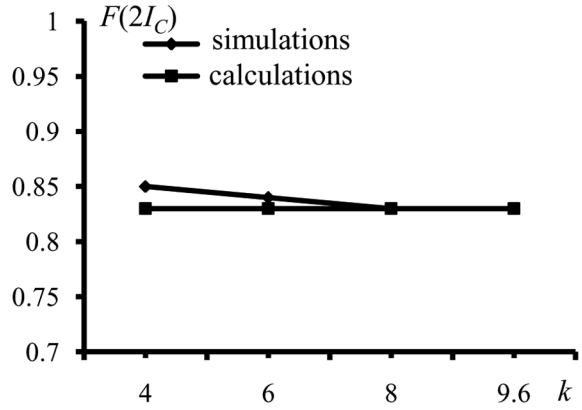

Fig. 7. Calculated versus simulated noise factor of the g_m-cell collector-current shot noise.

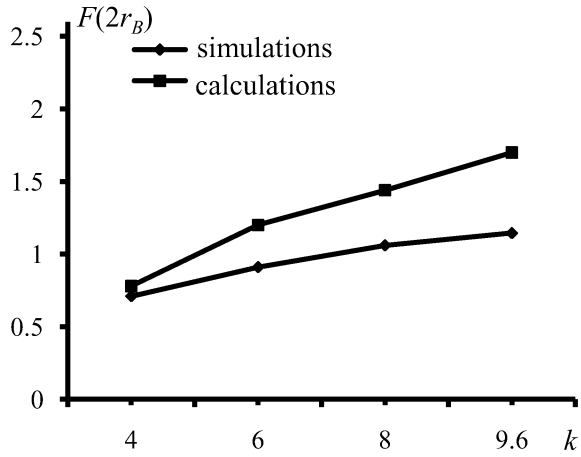

Fig. 8. Calculated versus simulated noise factor of the g_m-cell base-resistance thermal noise.

The calculated noise factor of the transconductor collector-current shot noise for bipolar *LC*-oscillators, (52), is compared with the simulation results in Fig. 7. A very good agreement has resulted.

The calculated and simulated noise factors of the transconductor base-resistance thermal noise [see (46)], the bias current source collector-current shot noise [$nk/2$ in (61)], and bias current source base-resistance thermal noise [nk^2c in (61)] are compared in Figs. 8, 9(a) and (b).

As observed from the diagrams, the calculated relationships between the noise factors and small-signal loop gain match those obtained from the simulations, thereby validating the phase noise model derived, i.e., (46), (52), (61), and (67).

As expected, the simulated small-signal loop-gain related contributions, Figs. 8, 9(a) and (b), account for around 70%–80% of the contributions obtained from the calculations for $k \gg 1$. As already explained in the previous section, the difference comes from the limited operational bandwidth of the devices and noise sources of the transconductor and bias

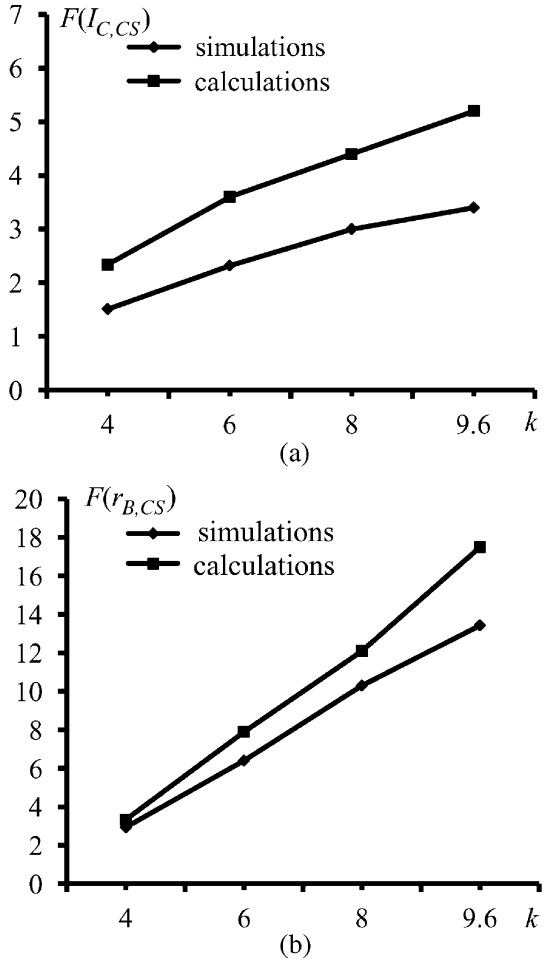

Fig. 9. Calculated versus simulated noise factor of bias current source (a) collector-current shot noise, (b) base-resistance noise.

current source as well as a finite transconductor switching time [6] accounted for in simulations (but not in calculations).

The match between the phase-noise simulated and calculated results depends on k, f_0, and operational bandwidth of the devices. The detail required to closely describe the small-signal loop-gain (and, hence, power-consumption) related contributions is adequately captured in modern computer-aided design tools.

The results of this comparative study verify the derived oscillator phase-noise model. Though overestimating the phase noise performance, the formulations derived are intuitive and give a valuable insight into the origin of phase noise in the *LC* oscillator under consideration. In the remainder of the paper we will refer to the formulations introduced while drawing conclusions impacting the design of *LC* oscillators.

B. Existing Phase-Noise Models for Bipolar LC-Oscillators

Numerous phase-noise analysis methods can be found in literature, among them frequency-domain, time-domain, linear, and nonlinear analyses. Linear frequency-domain analysis assumes that noise is superimposed directly onto the carrier [1]. Another way to use linear analysis in the frequency domain is to consider the noise sources to be additive to the phase of the carrier [2], [3]. Similarly, noise added to the phase [4]–[6] and carrier [7], [8] in the time domain has been used for phase-noise modeling in oscillators. Some of these methods have provided closed-form expressions for the oscillator phase noise [16], [20]–[22].

The observations made in this paper agree with the findings in [6] that provides expressions for the noise factors of the g_m-cell base-resistance thermal noise and the bias current source collector-current shot noise. To account for a finite bandwidth of operation of the oscillator devices and noise sources, empirical parameters are added to the corresponding noise factors in [6]. The results of this paper, however, provide an intuitive, closed-form formulation for the phase noise, while using electrical circuit parameters.

The results of the phase-noise analysis applied to CMOS *LC*-oscillators can be found elsewhere [5], [16]–[20], lending themselves to use in hand calculations and computer-aided design.

Note that the results in [5], [6], [12], [15]–[20] refer to hard-switching oscillators where transconductors operate for a large portion of the oscillation period in the limiting region.

VI. Test Oscillator Design

A test oscillator shown in Fig. 10(a) has been designed that support the 802.11a, HiperLAN2, and 802.16a standards [23]–[25], operating in the upper 5 GHz-range band. The test circuit of the shown bipolar *LC*-VCO is used for *verification* of the phase-noise model derived using the spectral noise analysis method. It consists of the symmetric *LC*-tank inductor L, two nMOS varactors C_V, feedback capacitors C_A and C_B, a cross-coupled transconductor $(Q_1 - Q_2)$, and a bias current source Q_{CS}. V_{CC} is the supply voltage, $V_{\rm TUNE}$ the varactor tuning voltage, V_B the base bias voltage, and $I_{\rm TAIL}$ the bias current.

A. Bipolar LC-Oscillator Circuit Parameters

The test oscillator bias and circuit parameters are optimized for the largest voltage swing (and k) around the 5.7 GHz central oscillation frequency, which allows for a comparison of the measured/simulated and calculated (modeled) phase-noise performance.

For a supply voltage of $V_{CC} = 2.2$ V, a transconductor base bias voltage V_B between 1.8-1.85 V has been chosen. It allows for both the largest voltage swing of the output signal and the most efficient use of the voltage headroom available, as obtained from the simulations. The maximum voltage swing is estimated from the saturation condition of the transconductor transistors, in order to avoid noise injection of the forward-biased base-collector junctions [15]. This is given by (71)

$$v_{S,B,\rm MAX} \leq 2\frac{V_{CC} - V_B + V_{BE} - V_{CE,\rm SAT}}{n+1} \qquad (71)$$

where V_{BE} is the forward base-emitter voltage, $V_{CE,\rm SAT}$ the collector-emitter saturation voltage, $v_{S,B,\rm MAX}$ the maximum voltage swing across the bases of the transconductor. For a capacitor divider ratio or around $n \sim 1.6$, $v_{S,B,\rm MAX}$ of around 0.68 V is expected, corresponding to a small-signal loop gain of around 10.

Compromising between good phase noise, low power consumption, and large frequency tuning range (aiming at the upper

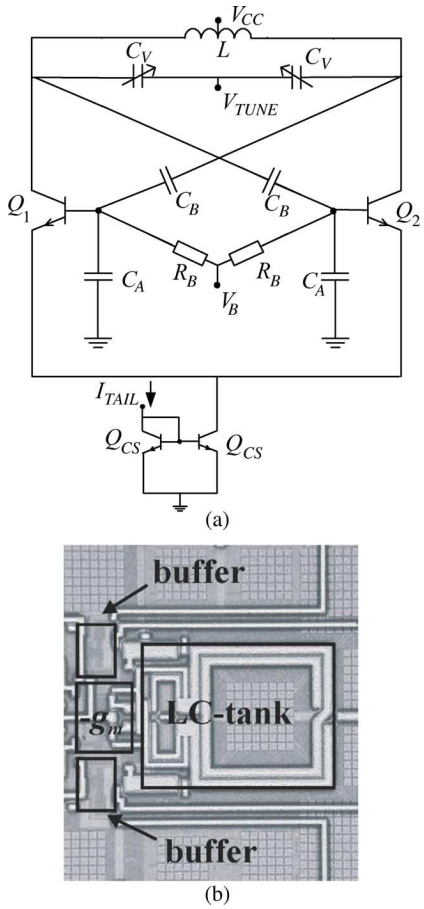

Fig. 10. Test bipolar *LC* voltage-controlled oscillator (a) schematic, (b) photomicrograph.

TABLE I
PHASE-NOISE PARAMETERS OF THE BIPOLAR *LC*-VCO SHOWN IN FIG. 10

parameter	value
G_{TK}	1/340S
n	1.6
k	10
c	0.25
L	1.2nH
C_B/C_A	250fF/100fF
f_0	5.7GHz

802.11a/HIPERLAN/802.16a band), the oscillator circuit parameters have been determined. The 1.2 nH symmetric and differentially shielded *LC*-tank inductor [L in Fig. 10(a)] has been designed using 4 um thick aluminum top metal. It has two turns, an outer dimension of 190 um, metal width of 10 um, and metal spacing of 5 um. Two n-type MOS varactors with 40 gates complete the *LC*-tank. Metal-insulator-metal capacitors C_A and C_B are 100 and 250 fF, respectively. Two common-collector output buffers interface the test oscillator and a 50 Ω measurement set-up, each consuming 1.1 mA of current. All the phase-noise relevant circuit parameters are overviewed in Table I.

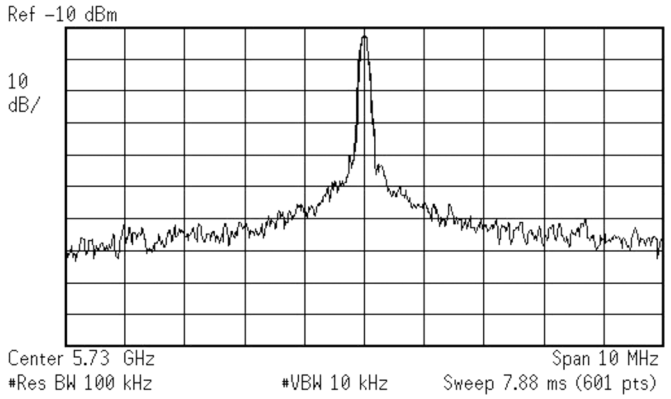

Fig. 11. Spectrum plot of the oscillation signal in the 5.7 GHz band for the bipolar *LC*-oscillator.

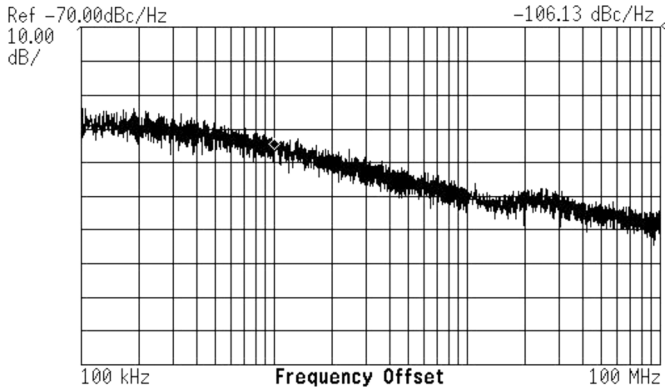

Fig. 12. Phase-noise plot of the test bipolar *LC*-oscillator in the 5.7 GHz band.

B. Experimental Results for the Bipolar LC-Oscillator

The chip photomicrograph of the core of the bipolar voltage-controlled oscillator designed is shown in Fig. 10(b). The oscillator core occupies an area of $215 \times 340\ \mathrm{um}^2$, including buffers. After wirebonding into 32-lead quad packages, the oscillator design was connected to a printed-circuit board with bias and supply line filtering for testing [15].

A frequency tuning range of 600 MHz (5.45 GHz–6.05 GHz) was measured for a 0.9 V tuning voltage range (i.e., between 1.3 and 2.2 V) [9]. The error in the prediction of the oscillation frequency is below 1%. This frequency tuning range covers the upper band of 802.11a/HIPERLAN/802.16a standards, and with additional MOS capacitors in parallel with the *LC*-tank the operating frequency could be trimmed to cover the complete 5 GHz band.

At around -12 dBm output power from a single buffer, the test oscillator achieves a phase noise of around -106 dBc/Hz at 1 MHz offset from the 5.7 GHz-band carrier for a current consumption of 4.8 mA and a 2.2 V supply voltage [9]. The spectrum and phase-noise plots of the oscillation signal are shown in Figs. 11 and 12.

As expected, the low phase-noise performance has resulted from the large contribution of noise from the bias current source that is shown in our phase-noise model to be much larger than all other phase-noise contributions (i.e., g_m-cell and *LC*-tank).

The overwhelming contribution of the BCS noise to the phase noise has already been confirmed by the extracted simulations of

Section V-A. The simulations show that for a small-signal loop gain of around 10, the BCS noise accounts for around 85%, the g_m-cell noise for around 10%, and the *LC*-tank noise for 5% of the phase-related noise power (the noise sources considered account for around 90% of the total phase noise).

Numerous noise-optimization procedures have been proposed that reduce noise generated by the *LC*-oscillator bias current source as the largest phase-noise contributor. As this topic attracts a lot of interest and a number of references can be found in the literature, we only make a brief mention of a result in [9], and refer to [10], [18], [26], [27] for a detailed treatment of other bias-current source noise reduction methods.

The phase-noise model derived in this paper has been used for the design of another *LC*-oscillator with the phase-noise contribution of the bias current source noise reduced. By forming a resonance in the emitter of the bias current source transistor at twice the oscillation frequency between an inductor and a base-emitter capacitor [9], a manifold phase noise improvement of the bipolar *LC*-oscillator under consideration can be realized: 6 dB better phase-noise has been measured from the bipolar *LC*-oscillator in [9] using this method, resulting in a phase noise of −112 dBc/Hz at 1 MHz offset from the 5.7 GHz-band carrier for a current consumption of 4.8 mA and a 2.2 V supply voltage, thereby satisfying the phase-noise requirements of the wireless communication standards in the 5 GHz upper frequency band.

C. Discussion of Experimental Results for the Bipolar LC-Oscillator

In this section we compare the measurement results to the results predicted by the oscillator phase-noise model derived in this paper and the extracted simulation results, for the bipolar *LC*-VCO.

For the extracted oscillator *LC*-tank parameters given in Section V-A, the results obtained from the phase-noise model, (67), and the results of simulations and measurement are compared for the largest small-signal loop gain in this section.

The result obtained from the phase-noise model is −107.4 dBc/Hz, the result of extracted simulations −108.6 dBc/Hz, and the result of measurements −106.1 dBc/Hz, all referring to 1 MHz offset from a 5.7 GHz carrier, and current consumption of 4.8 mA.

For the oscillator bias chosen, the simulations predict the best phase noise for a bias current of 4.8 mA. However, the best phase noise of the oscillator has been measured at around 5.4 mA, expectedly due to a lower than estimated Q-factor of the *LC*-tank. Correcting for the difference in *LC*-tank conductance, voltage swing, and noise factor between the measurements and simulations (i.e., accounting for a lower Q-factor of the *LC*-tank, lower voltage swing, and lower noise factor), calculations and simulations predict a phase noise of around −106.4 dBc/Hz and −107.6 dBc/Hz at 1 MHz offset from the 5.7 GHz-band carrier, respectively.

For the difference between the measurement and simulation results we may point to the difference in the estimated *LC*-tank parameters. The noise contributed by the base-current shot noise and base bias circuitry of the transconductor as well as the noise of the diode-connected bias current source transistor, which have not been taken into account in the phase-noise model, are another sources of difference. The noise sources considered account for around 90% of the total phase noise, as obtained from the simulations. As already discussed in Section IV-F, the difference between the calculation and simulation results originates from the limited operational bandwidth of the oscillator devices, not accounted for in the phase-noise model developed in this paper. Minor noise sources not considered in the analysis contribute to the difference as well.

The results of the comparative calculation/simulation study have demonstrated the validity of the phase-noise model derived. The formulations derived are intuitive and give insight into the origin of phase noise in bipolar *LC*-oscillators. They are amenable for design as they describe the oscillator phase-noise performance using electrical circuit parameters.

The measurement results of this section, the simulation results of Section V-A, and the comparative study with the results found in literature of Sections V-B, verify the oscillator phase-noise models of (67) derived for the bipolar *LC*-VCO shown in Fig. 2.

VII. Conclusion

We have used spectral noise analysis to derive an intuitive and complete phase-noise formulation for bipolar *LC* voltage-controlled oscillators. A phase-noise model of hard-switching bipolar *LC*-oscillators has been developed as a function of the oscillator circuit parameters. The results obtained from the rigorous phase-noise analyses are valuable to oscillator designers, describing how phase noise is generated in *LC*-oscillators.

The contributions of all noise sources to the phase noise of the bipolar *LC* voltage-controlled oscillators have also been determined. It has been shown that the contribution of the bias current source noise to the phase noise is larger than all other noise contributions put together, a factor of around the small-signal loop gain.

The validity of the phase-noise model derived has been tested by comparing the model predictions with the results obtained from the simulations and measurements of the bipolar *LC*-oscillator designed. The phase-noise model developed in this paper compares favorably with other models found in literature.

References

[1] J. Craninx and M. Steyaert, "Low-noise voltage-controlled oscillators using enhanced LC-tanks," *IEEE Trans. Circuits Syst. II, Exp. Briefs*, vol. 42, no. 12, pp. 792–804, Dec. 1995.
[2] D. B. Leeson, "A simple model of feedback oscillator noise spectrum," *Proc. IEEE*, vol. 54, no. 2, pp. 329–330, Feb. 1966.
[3] G. Sauvage, "Phase noise in oscillators: A mathematical analysis of Leeson's model," *IEEE Trans. Instrum. Meas.*, vol. IM-26, no. 4, pp. 408–410, Dec. 1977.
[4] W. Robins, *Phase Noise in Signal Sources*. London, U.K.: Peter Peregrinus Ltd, 1982.
[5] A. Hajimiri and T. H. Lee, "A general theory of phase noise in electrical oscillators," *IEEE J. Solid State Circuits*, vol. 33, no. 2, pp. 179–194, Feb. 1998.
[6] C. Samori, A. Lacaita, F. Villa, and F. Zappa, "Spectrum folding and phase noise in LC tuned oscillators," *IEEE Trans. Circuits Syst.*, vol. 45, no. 7, pp. 781–790, Jul. 1998.
[7] E. Hafner, "The effect of noise in oscillators," *Proc. IEEE*, vol. 54, no. 2, pp. 179–198, Feb. 1966.

[8] A. van der Ziel, *Noise in Solid-State Devices and Circuits*. New York: Wiley-Interscience, 1986.
[9] A. Tasić, W. A. Serdijn, J. R. Long, and D. Harame, "Resonant-inductive degeneration for a fourfold phase-noise improvement of a 5.7 GHz band voltage-controlled oscillators," in *Proc. IEEE Bipolar/CMOS Circuit Technol. Meet.*, Oct. 2005, pp. 236–239.
[10] E. Hegazi, H. Sjoland, and A. Abidi, "Filtering technique to lower oscillator phase-noise," in *Proc. ISSCC*, Feb. 2001, pp. 364–365.
[11] W. R. Bennett, "Methods of solving noise problems," in *Proc. IRE*, May 1956, pp. 609–637.
[12] L. W. Couch, II, *Digital and Analog Communication Systems*. Upper Saddle River, NJ: Prentice-Hall, 1997, 07458.
[13] Q. Huang, "Phase noise to carrier ratio in LC oscillators," *IEEE J. Solid State Circuits*, vol. 47, no. 7, pp. 965–980, Jul. 2000.
[14] C. A. M. Boon, "Design of high-performance negative feedback oscillators," Ph.D. dissertation, Dept. Microelectron., Delft Univ., Delft, The Netherlands, 1989.
[15] A. Tasić, W. A. Serdijn, and J. R. Long, "Design of multi-standard adaptive voltage-controlled oscillators," *IEEE Trans. Microw. Theory Techn.*, vol. 53, no. 2, pp. 556–563, Feb. 2005.
[16] J. Rael and A. Abidi, "Physical processes of phase noise in differential LC oscillators," in *Proc. CICC*, Sep. 2000, pp. 569–572.
[17] E. Hegazi, J. Rael, and A. Abidi, *The Designers Guide to High-Purity Oscillators*. Norwell, MA: Kluwer, 2005.
[18] A. Hajimiri and T. Lee, "Design issues in CMOS differential LC oscillators," *IEEE J. Solid State Circuits*, vol. 34, no. 5, pp. 717–724, May 1999.
[19] P. Andreani and A. Fard, "A 2.3 GHz LC-tank CMOS VCO with optimal phase-noise performance," in *Proc. ISSCC*, Feb. 2006, pp. 194–195.
[20] P. Andreani, X. Wang, L. Vandi, and A. Fard, "A study of phase noise in colpitts and LC-tank CMOS oscillators," *IEEE J. Solid State Circuits*, vol. 40, no. 5, pp. 1107–1118, Mar. 2005.
[21] A. Jerng and C. G. Sodini, "The impact of device type and sizing on phase noise mechanisms," *IEEE J. Solid State Circuits*, vol. 40, no. 2, pp. 360–369, Feb. 2005.
[22] A. Fard and P. Andreani, "An analysis of $1/f^2$ phase noise in bipolar colpitts oscillators (with a digression on bipolar differential pair LC oscillators)," *IEEE J. Solid State Circuits*, vol. 42, no. 2, pp. 374–384, Feb. 2007.
[23] "The IEEE 802.16 working group on broadband wireless access standards," [Online]. Available: http://www.ieee802.org/16/
[24] "ETSI HIPERLAN/2 Standard," 2006. [Online]. Available: http://portal.etsi.org/bran/kta/Hiperlan/hiperlan2.asp
[25] *Wireless LAN MAC and Physical Layer (PHY) Specification—High-Speed PHY in the 5 GHz Band*, ANS/IEEE Standard 802.11a, 1999.
[26] P. Andreani and H. Sjoland, "Tail current noise suppression in RF CMOS VCOs," *IEEE J. Solid State Circuits*, vol. 37, no. 3, pp. 342–348, Mar. 2002.
[27] A. Tasić, W. A. Serdijn, and J. R. Long, *Adaptive Low-Power Circuits for Wireless Communications*. New York: Springer, 2006.

Aleksandar Tasić received the M.Sc. degree in electronics and telecommunications from the Electronics Faculty, University of Nis, Nis, Serbia, in 1998, and the Ph.D. degree from the Faculty of Electrotechnics, Mathematics, and Informatics, the Delft University of Technology, Delft, the Netherlands, in 2005.

Between 1998 and 2000, he was a Research Assistant with the Electronics Faculty, University of Nis. Between 2005 and 2007, he was working as an Assistant Professor at the Electronics Research Laboratory/DIMES, the Delft University of Technology. In 2005/2006, he was appointed as a Visiting Research Scientist at the University of California, San Diego. Since 2007, he has been with Qualcomm, San Diego, CA, first as a Senior and then as a Staff RF/Analog Engineer. His research interest includes design of adaptive and multistandard receiver circuits and systems for wireless communications.

Wouter A. Serdijn was born in Zoetermeer ("Sweet Lake City"), the Netherlands, in 1966. He received his "ingenieurs" (M.Sc.) degree from the Faculty of Electrical Engineering and the Ph.D. degree from the Electronics Research Laboratory, the Delft University of Technology, Delft, the Netherlands, in 1989 and 1994, respectively.

His research interests include low-voltage, ultra-low-power, high-frequency and dynamic-translinear analog integrated circuits along with circuits for RF and UWB wireless communications, hearing instruments and pacemakers. He teaches Analog Electronics for Electrical Engineers, Micropower Analog IC Techniques and Electronic Design Techniques. He has authored and coauthored more than 150 publications and presentations.

Dr. Serdijn has served as an Associate Editor for the IEEE TRANSACTIONS ON CIRCUITS AND SYSTEMS—II: EXPRESS BRIEFS, as chair of the Analog Signal Processing Technical Chapter of the IEEE CAS society, and currently serves as an Associate Editor for the IEEE TRANSACTIONS ON CIRCUITS AND SYSTEMS—I: REGULAR PAPERS.

John R. Long received the B.Sc. degree in electrical engineering from the University of Calgary, Calgary, AB, Canada, in 1984, and the M.Eng. and Ph.D. degrees in electronics engineering from Carleton University, Ottawa, ON, Canada, in 1992 and 1996, respectively.

He was employed for 10 years by Bell-Northern Research, Ottawa, ON, Canada, where he was involved in the design of ASICs for Gbit/s fiber-optic transmission systems and for 5 years at the University of Toronto, Toronto, ON, Canada. He joined the faculty at the Delft University of Technology, Delft, The Netherlands, in January 2002 as Chair of the Electronics Research Laboratory. His current research interests include: low-power transceiver circuitry for highly-integrated radio applications, and electronics design for high-speed data communications systems.

Prof. Long is currently serving on the Technical Program Committees of the International Solid-State Circuits Conference (ISSCC), the European Solid-State Circuits Conference (ESSCIRC), the IEEE Bipolar/BiCMOS Circuits and Technology Meeting (BCTM), and GAAS2004 (EuMW). He is a former Associate Editor of the IEEE JOURNAL OF SOLID-STATE CIRCUITS. He was a recipient of the NSERC Doctoral Prize and Douglas R. Colton and Governor General's Medals for research excellence, and Best Paper Awards from ISSCC 2000 and IEEE-BCTM 2003.